RESEARCH ARTICLE | MAY 11 2026

Temperature-dependent capacitance of the electrical double layer

Ole Nickel ; Mathijs Janssen ; Alexander Schlaich ; Robert Horst Meißner

J. Chem. Phys. 164, 184703 (2026)
https://doi.org/10.1063/5.0318194

The Journal of Chemical Physics ARTICLE pubs.aip.org/aip/jcp

Temperature-dependent capacitance of the electrical double layer

Cite as: J. Chem. Phys. 164, 184703 (2026); doi: 10.1063/5.0318194
Submitted: 19 December 2025 • Accepted: 9 April 2026 •
Published Online: 11 May 2026

Ole Nickel,[1,2] Mathijs Janssen,[3] Alexander Schlaich,[4] and Robert Horst Meißner[1,2,a)]

AFFILIATIONS

[1] Institute for Interface Physics and Engineering, Hamburg University of Technology, Hamburg, Germany
[2] Institute of Surface Science, Helmholtz-Zentrum Hereon, Geesthacht, Germany
[3] Institute of Physics, Norwegian University of Life Sciences, Ås, Norway
[4] Institute for Physics of Functional Materials, Hamburg University of Technology, Hamburg, Germany

[a)] **Author to whom correspondence should be addressed:** robert.meissner@tuhh.de

ABSTRACT

We use atomistic simulations to study the electrical double layer (EDL) at an electrode–electrolyte interface at different temperatures. For a constrained electrode charge, the potential drop over the EDL increases with temperature, a phenomenon known as the thermal voltage rise (TVR). Prior continuum models attributed TVR to expansion of the EDL with increasing temperature; conversely, our simulations with aqueous, organic, and ionic liquids show that the EDL does not expand but that the TVR is caused by a decrease in interfacial permittivity with increasing temperatures.

I. INTRODUCTION

The performance of supercapacitors, batteries, and other electrochemical energy storage and generation devices relies heavily on the behavior of electrolytes near charged electrode surfaces. There, electric double layers (EDLs) form, which comprise electronic surface charge and ionic charges in the electrolyte. For a given electrode surface charge, the structure of the EDL dictates the potential drop at the electrode surface and, hence, its capacitance. Upon varying an electrochemical device's temperature, its EDL structure changes, and so will the device's capacitance. Such temperature dependence in an electrochemical device's capacitance might be used to convert waste heat into electricity via a thermal capacitive electrochemical cycle (TCEC). In a TCEC, a capacitor is charged and discharged at different temperatures, analogous to heat-engine cycles with compression and expansion at different temperatures.[1–6] Experiments on aqueous and organic electrolytes have shown that, for a fixed surface charge, the electrode potential rises with increasing temperature: this effect is known as thermal voltage rise (TVR) (or equivalently, a decrease in capacitance with increasing temperature).[1–3,5,7–9] Conversely, in experiments on ionic liquids, both increasing[10–14] and decreasing[15–17] capacitance with increasing temperature were observed. The increase in capacitance for ionic liquids is related to weaker ion association at higher temperatures, which allows structural changes at the interface to improve the screening of the potential by the ions.[11,18] A recent study[5] pointed out that the increased self-discharge at high temperatures limits the feasibility of the TCEC. To make TCEC technologically feasible, electrode–electrolyte combinations must be found whose EDL capacitance responds the strongest to variations in temperature. Accordingly, a better understanding of the temperature dependence of electric double layers (EDLs) is crucial.

The structure and formation of the EDL have been studied continuously since the pioneering work by Helmholtz, who treated the EDL as a parallel-plate capacitor with its surface charge screened by a compact layer of ions of opposite charge at an atomic distance from the electrode. Instead, Gouy and Chapman realized that thermal motion at a finite temperature will drive ions somewhat from the electrode, resulting in a diffuse EDL (GC model).[19] Solving the Poisson–Boltzmann equation for a flat electrode and a semi-infinite electrolyte, Gouy and Chapman found that the potential drops across the diffuse layer by[20,21]

$$\Psi_{GC} = \frac{2k_B T}{e} \sinh^{-1}\left(\frac{\sigma}{\sqrt{8\varepsilon_0 \varepsilon_r k_B T \rho_s}}\right), \quad (1)$$

where k_B is the Boltzmann constant, T is the temperature, e is the elementary charge, σ is the surface charge density, ε_0 is the vacuum permittivity, ε_r is the relative permittivity, and ρ_s is the ion concentration. Ψ_{GC} in Eq. (1) depends on the temperature explicitly in two places, and implicitly through the temperature dependence of the relative permittivity. For a fixed charge and ignoring the temperature dependence of ε_r, Ψ_{GC} rises with increasing temperature, the TVR, in qualitative agreement with several experiments of both aqueous[1,9] and organic electrolytes.[3,5]

To interpret the origin of the TVR, we can write the GC model's capacitance as

$$C_{GC} = \frac{\sigma A}{\Psi_{GC}} = \frac{\varepsilon_0 \varepsilon_r A}{L_{eff}}, \quad (2)$$

where A is the electrode surface area, L_{eff} is an effective EDL width,[21] and

$$L_{eff} = \frac{2k_B T \varepsilon_0 \varepsilon_r}{e\sigma} \sinh^{-1}\left(\frac{\sigma}{\sqrt{8\varepsilon_0 \varepsilon_r k_B T \rho_s}}\right), \quad (3)$$

which reduces to the Debye length for $\sigma \ll \sqrt{8\varepsilon_0 \varepsilon_r k_B T \rho_s}$. With an increase in salt concentration, L_{eff} decreases and C_{GC} increases.[21,22] The concentration dependence of C_{GC} can be utilized to harvest "blue energy" in thermodynamic charging–discharging cycles at different salinities, for instance, between sea and river water.[21,23–26] In the same way, one can consider how L_{eff} varies with temperature. For a temperature-independent permittivity, Eq. (2) shows that capacitance decreases as the effective diffuse layer thickness increases with rising temperature. This led different studies[3,5,7,9] to link thermal energy harvesting to thermal EDL expansion. However, using experimental data for $\varepsilon_r(T)$, the diffuse EDL shrinks even though the voltage rises.[27] Ahualli *et al.*[1] explained the temperature dependence of the capacitance by a change in the solvent's permittivity, naming the phenomenon "Double Layer Permittivity Exchange."

Despite its popularity and successes, the GC model has several well-documented limitations. It ignores the electrode's atomic structure and treats the solvent as a homogeneous dielectric continuum.[19] Moreover, the GC model treats ions as point charges with mean-field Coulomb ion–ion interactions and, accordingly, cannot describe electrolytes in nanoconfinement, subject to large potentials, or multivalent or concentrated electrolytes.[19] In this work, we find again that GC predictions are far from molecular dynamics (MD) simulations, especially for concentrated electrolytes and near highly charged electrodes, where ionic steric interactions are important and violate GC's point ion assumption. As a first step to incorporate finite ionic size, Stern combined the compact and diffuse layers into the Gouy–Chapman–Stern (GCS) model, as shown in Fig. 1.[28] By using different permittivities in the compact and diffuse layers, one can account for solvent structure and ion adsorption in the compact layer.[29] However, using bulk values of ε_r in the mean-field GCS theory is an oversimplification because the permittivity of solvents can vary drastically at interfaces and in nanoconfinement.[30–35] Like the GC model, for a temperature-independent permittivity, the GCS qualitatively predicts the electrode potential to increase monotonously with increasing temperature.

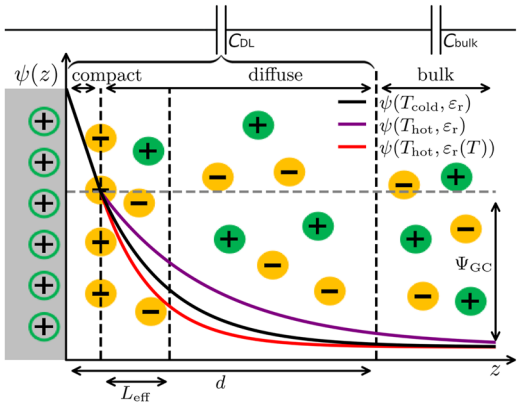

FIG. 1. Schematic of the Stern model, which describes the EDL with a compact and a diffuse layer of ions.

More recent theoretical studies model the electrical double layer using size-modified mean field theory,[8,26] continuum simulations with implicit solvents,[36–39] and classical density functional theory.[2,40] Some of these works attributed the TVR to increased thermal motion of ions and associated changed in entropy, rather than to changes in the permittivity or double-layer width.[2,39,41] Consistent with experimental results, these studies predicted the capacitance to decrease with increasing temperatures. However, we note that all EDL models described above treated the solvent implicitly, as a dielectric background. The solvent is known to play an essential role in EDL structure and, therefore, presumably, also in its temperature dependence. Yet, insight into the effect of the EDL's atomistic structure on the temperature dependence of its capacitance is lacking.[42]

Here, we use all-atom molecular simulations to study the structure of the EDL at different temperatures. As will be demonstrated, our MD predictions for the TVR are in qualitative agreement with experimental data; this is to be contrasted with GC-type models that typically reveal larger discrepancies. We analyze our simulations in terms of spatially varying permittivity and associated interfacial permittivity, ε_{DL}, which accounts for solvent and ion effects at the electrode-electrolyte interface.

II. METHODS

A. Simulation details

The June 2022 version of LAMMPS[43] was used to perform molecular dynamics (MD) simulations of a model supercapacitor containing different electrolytes between two flat electrodes, consisting of three graphite layers each. We use a Cartesian coordinate system where the electrodes are parallel to the *xy* plane. Parameters for carbon atoms in graphite were taken from Cheng and Steele.[44] The surface charge density σ was controlled using the constrained charge method of the electrode package.[45] The distance between the electrodes determines the density of the liquids and is adjusted depending on the temperature by applying constant atmospheric pressure to one electrode during an equilibration run. In the production runs, the electrode positions are fixed.

Three different electrolytes were investigated: one aqueous, one organic, and one ionic liquid. The aqueous electrolyte was composed of 3240 SPC/E[46] water molecules and 58 ion pairs of KCl, giving a concentration of 1M. Parameters for KCl were taken from Deublein, Vrabec, and Hasse.[47] The water molecule's bonds and angles were held rigid using the shake algorithm.[48] The organic electrolyte consisted of 1608 acetonitrile (ACN) molecules and 84 ion pairs of TEA-BF_4, giving a concentration of 1M. The parameters for ACN were taken from Price, Ostrovsky, and Jorgensen,[49] and the CL&P force field[50] was used for the ions. Simulations with a pure ionic liquid contained 1720 ion pairs of BMIM-PF_6, which were described using a coarse-grained force field.[51] Arithmetic mixing rules were used to determine the mixing of Lennard-Jones parameters. Electrostatic interactions were computed with a PPPM solver optimized for constant charge simulations[52] with a (relative) accuracy setting of 10^{-6}. The systems were periodic in the electrode plane and non-periodic in the direction normal to the electrodes; therefore, the commonly employed Yeh–Berkowitz correction for slab geometries was used.[53] The temperature of the electrolyte was set by global velocity rescaling with Hamiltonian dynamics.[54] Several replicas with random starting positions were run for each temperature. Additional simulation parameters (including surface charge density, temperature, and simulation time) are presented in Sec. S2 in the supplementary material.

B. Calculation of the interfacial capacitance

The potential along the z direction is calculated from the electrolyte charge density $\rho_{el}(z)$ as

$$\psi(z) = -\frac{1}{\varepsilon_0}\int_{-L/2}^{z}\int_{-L/2}^{z'}\rho_{el}(z'')\mathrm{d}z''\mathrm{d}z'. \tag{4}$$

The latter was averaged and binned with a resolution of 0.01 Å within LAMMPS during the simulation. The potential difference Ψ between the electrodes at the positions $z = \pm L/2$ is obtained from $\Delta\psi = \psi(L/2) - \psi(-L/2)$.

For a pure dielectric—meaning there are no free charges (ions)—the corresponding response function simply is the solvent's (inverse) dielectric permittivity.[55] Unlike charge-free solvents, electrolytes have a dielectric contribution from molecular rotations of the solvent (and possibly ions) and an additional contribution from ion transport. Thus, in the case of electrolytes, one defines a "generalized dielectric constant" that describes the electrostatic screening of the entire electrolyte, i.e., solvent and ions.[56] The generalized inverse dielectric response function $\varepsilon^{-1}{}_{\perp}(z)$ in the presence of ions is defined through

$$\Delta E_{\perp}(z) = \frac{\Delta D_{\perp}^{\mathrm{ext}}}{\varepsilon_0}\varepsilon^{-1}{}_{\perp}(z), \tag{5}$$

where $\Delta E_{\perp}(z)$ is the difference in electric field between uncharged and charged electrodes and $\Delta D_{\perp}^{\mathrm{ext}}$ is the corresponding difference in the external displacement field, accounting only for the electrode charges. In our flat-plate geometry, $\Delta D_{\perp}^{\mathrm{ext}} = \sigma$.

The electrical field response can be calculated using the constitutive equation for electric fields and the polarization response of the electrolyte,

$$\Delta E_{\perp}(z) = \varepsilon_0^{-1}[\Delta D_{\perp}^{\mathrm{ext}} - \Delta P(z)], \tag{6}$$

where $\Delta P(z) = m_{\perp}(z) - m_{\perp,0}(z)$ is the polarization density difference of the electrolyte. Here,

$$m_{\perp}(z) = -\int_0^z \rho_{el}(z')dz' \tag{7}$$

is the local polarization density with an applied external field (i.e., charged electrodes), $m_{\perp,0}(z)$ is the local polarization density without an external field (i.e., uncharged electrodes), and ρ_{el} is the charge density of the electrolyte. Combining Eqs. (5) and (6) yields the inverse permittivity profile from simulations with applied fields,[35,57]

$$\varepsilon_{\perp}^{-1}(z) = \frac{\Delta D_{\perp}^{\mathrm{ext}} - \Delta P(z)}{\Delta D_{\perp}^{\mathrm{ext}}} = 1 - \frac{\Delta P(z)}{\Delta D_{\perp}^{\mathrm{ext}}}. \tag{8}$$

The profile can be integrated over a defined interface width, d. Ideally, d is chosen such that the complete potential is screened (see Fig. 1). The interfacial permittivity is then obtained from

$$\varepsilon_{\mathrm{DL}} = \frac{d}{\int_0^d \varepsilon_{\perp}^{-1}(z)\,dz}. \tag{9}$$

From this, the interfacial capacitance follows directly by assuming that the EDL resembles a plate capacitor,

$$C_{\mathrm{DL}} = \varepsilon_0\varepsilon_{\mathrm{DL}}\frac{A}{d}, \tag{10}$$

where A is the electrode surface area. Equation (10) is similar to Eq. (2) and can also be found in Pandolfo and Hollenkamp.[58] An equivalent circuit that reproduces the capacitance of the complete cell can be found in Fig. S1 of the supplementary material. circuit includes a that can be Equation (10) deviates from the usual mean-field assumption of constant permittivity throughout the cell and takes into account the local electrolyte structure at the interface. Here, d is chosen for each electrolyte individually and is the point at which approximately no layering is observed anymore [for KCl shown in Fig. 3(a) with a black dashed line].

III. RESULTS

A. Thermal voltage rise

TCEC performance depends on the thermal voltage rise, $\Delta\Psi = \Psi_{\mathrm{hot}} - \Psi_{\mathrm{cold}}$, where Ψ_{hot} and Ψ_{cold} are the potential differences between electrodes at different temperatures but with the same surface charge density σ. Throughout this article, we use T_{cold} = 293 K and T_{hot} = 373 K. The ratio of Ψ_{hot} and Ψ_{cold}, denoted by α_{Ψ}, is equivalent to the ratio of the capacitance of the hot and cold systems,

$$\alpha_{\Psi} = \frac{C_{\mathrm{cold}}}{C_{\mathrm{hot}}} = \frac{\Psi_{\mathrm{hot}}}{\Psi_{\mathrm{cold}}}, \tag{11}$$

which relates the relative increase in capacitance to the TVR. To measure the TVR, simulations were performed using a constant surface charge on the electrodes. Specifically, we made all three graphitic layers of each electrode polarizable. The surface charge density on the electrodes of $\sigma = 0.21$ e/nm^2 for KCl, $\sigma = 0.32$ e nm^{-2} for TEA-BF$_4$, and $\sigma = 0.45$ e nm^{-2} for BMIM-PF$_6$ were chosen such that the potential between the electrodes lies within the electrolyte's electrochemical window. At the lowest temperature ($T_{\text{cold}} = 293$ K), the potential between the electrodes was around 1 V for KCl, 2 V for TEA-BF$_4$, and 3 V for BMIM-PF$_6$. For comparison, we report the GC model predictions [Eq. (1)] for that temperature and surface charge densities. Since Eq. (1) describes only a single EDL, the values reported in this section are doubled to enable direct comparison with the cell potential. For $\rho_s = 1$ mol/l and $\epsilon_r = 72$ (taken from bulk simulations of SPC/E water[59]), we find $\Psi_{\text{GC,KCl}} = 29.5$ mV; for $\rho_s = 1$ mol/l and $\epsilon_r = 35$ (taken from Ref. 60), we find $\Psi_{\text{GC,TEA-BF}_4} = 62$ mV; for $\rho_s = 4.8$ mol/l and $\epsilon_r = 14$ (taken from Ref. 61), we find $\Psi_{\text{GC,BMIM-PF6}} = 74$ mV. Hence, the GC model underestimates electrode potentials by more than an order of magnitude.

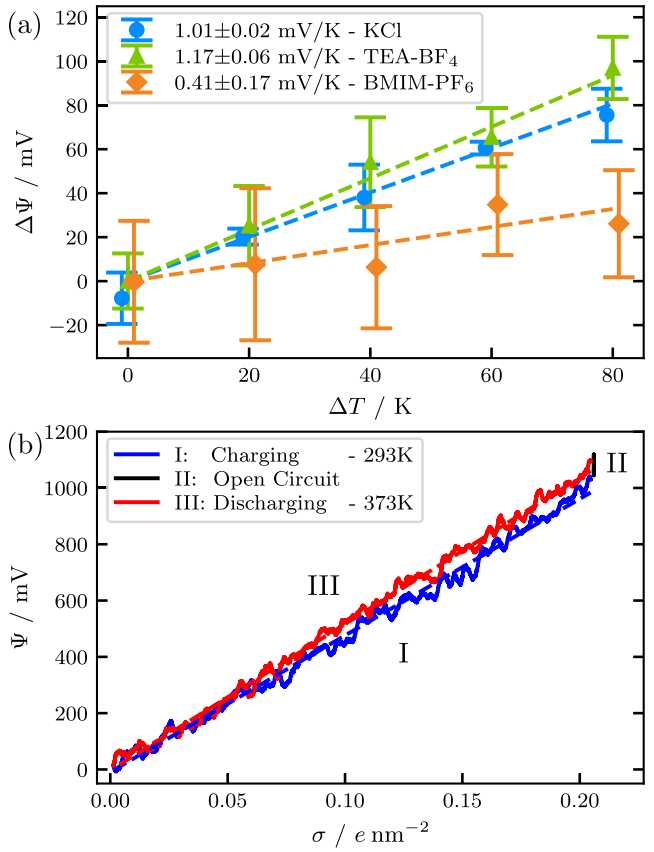

FIG. 2. (a) Potential change $\Delta\Psi$ of a charged supercapacitor with different electrolytes, when the temperature is increased by ΔT. $\sigma = 0.21$ e nm for KCl, $\sigma = 0.32$ e nm for TEA-BF$_4$, and $\sigma = 0.45$ e nm for BMIM-PF$_6$ is used. The x axis is shifted by 1 K between electrolytes for better visibility. (b) Simulated TCEC cycle with KCl, where the cell is charged at low temperature and discharged at high temperature. The running average over 0.2 ns is plotted for better visibility.

The TVR is plotted against the temperature difference ΔT in Fig. 2(a). For all electrolytes, the TVR increases linearly with the temperature difference, indicating that temperature sensitivity is a general EDL phenomenon. The temperature sensitivity of the potential, $(\Delta\Psi/\Delta T)_\sigma$, was obtained for the different electrolytes via a linear fit, whose slopes and their standard errors are reported in Fig. 2(a). The standard error is calculated from the square root of the diagonal element in the covariance matrix of the fit. The value for TEA-BF$_4$ is reasonably close to the experimental value of 0.63 mV/K for a commercial supercapacitor.[2,3,62] For an aqueous electrolyte with 1M KNO$_3$, Wang *et al.*[9] found $(\Delta\Psi/\Delta T)_\sigma = 0.44$ and 0.66 mV/K, depending on the electrode material used, which is in the same range as our estimate for 1M KCl. The results for both electrolytes are reasonably consistent with previous results and suggest that the temperature dependence of the EDL can be reproduced, at least qualitatively, using MD simulations. Again, GC predictions are far off. For the aqueous KCl electrolyte, inserting T_{hot} and the corresponding $\epsilon_r = 51$ into Eq. (1) gives $\Psi_{\text{GC}} = 39.5$ mV. In turn, we find $\Delta\Psi_{\text{GC}}/\Delta T = (39.5–29.5\text{ mV})/80\text{ K} = 0.12$ mV/K, much lower than observed in the experiments and simulations.

B. Thermal capacitive electrochemical cycle

Next, we replicate a TCEC in our MD simulations by (I) charging the supercapacitor with a constant current, (II) raising the cell's temperature at a constant charge, and (III) discharging the supercapacitor with a constant current at the high temperature. The resulting cycle is shown for 1M KCl in Fig. 2(b). We observe that, for the used parameters, the potential between the electrodes, Ψ, depends linearly on the surface charge density, σ; hence, the capacitance is constant during charging and discharging. The electric energy generated by the TCEC corresponds to the area enclosed by the blue, red, and black lines in Fig. 2(b) and can be calculated via the integral $W/A = (1/A)(\int\Psi_{\text{hot}}(t)I\,\mathrm{d}t - \int\Psi_{\text{cold}}(t)I\,\mathrm{d}t) = 8.4$ meV/nm^2, where I is the electric current.

Because the capacitance remains constant during charging and discharging, the temperature sensitivity $(\Delta\Psi/\Delta T)_\sigma$, which is the difference in potential between phases I and III [see Fig. 2(b)], must increase linearly with the surface charge. Thus, the system should be charged as much as possible before raising the temperature to maximize electric energy output. Using the TVR, the electric energy can also be obtained as $\Delta W/A = 0.5 \cdot \sigma(\Psi_{\text{hot}} - \Psi_{\text{cold}}) = 8.5$ meV/nm^2. Comparing the electric energies obtained from direct TCEC and independent TVR simulations, we conclude that MD simulations at constrained charge can replicate the entire TCEC process, as both values are in good agreement. It should be noted that it is unnecessary to simulate computationally expensive cycles, as the relevant TVR can be obtained directly from cheaper simulations at a constant electrode charge. Simulating a full TCEC cycle might be interesting when the capacitance is not constant with respect to the surface charge, which can occur with some ionic liquids[63] or porous electrodes.[64]

C. Charge density profile of the EDL

To understand the impact of the structural changes that occur in the EDL on the TVR, we examine how the charge density and potential profiles change when the system is heated. Figure 3(a) shows MD simulation data for the electrolyte charge density near the

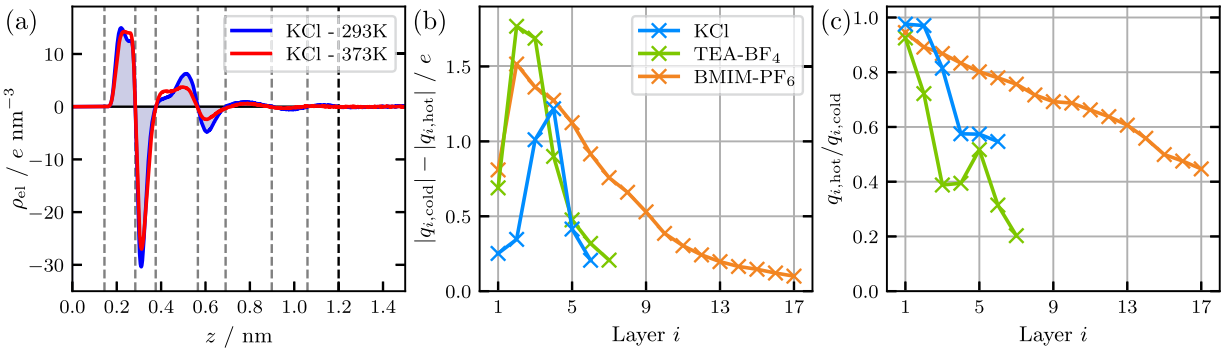

FIG. 3. (a) Charge density profile for KCl with the negative electrode on the left. The vertical gray dashed lines indicate the different layers, and the blue shaded area is the amount of charge in that layer. The vertical black dashed line show the interface width d. (b) Absolute reduction in charge from temperature increase for each layer on the negative electrode. (c) Relative reduction in charge for each layer as a ratio between the hot and cold interface.

left electrode for KCl at T_{hot} and T_{cold}. We observe alternating layers of opposite charge due to ions and solvent molecules adsorbing at specific distances and orientations on the surface—this is to be contrasted with the GCS model, which predicts charge densities to decay monotonously instead. The peak height decreases with temperature, suggesting that the EDL becomes more disordered.

We were unable to find an intuitive definition for the EDL width from our atomistic simulations that correlates with capacitance. Generally, one may define the EDL width by the first moment of its charge density, $\lambda = \int_0^\infty z\rho_{el}(z)dz / \int_0^\infty \rho_{el}(z)dz$. This definition works well with solutions to Poisson–Boltzmann-type continuum models (Debye–Hückel, Gouy–Chapman, etc.), whose charge and potential profiles decay exponentially away from an electrode surface, and for which λ will reduce to the Debye length, or potential-modified versions thereof. However, for our MD simulations, λ is impractical, as small charge fluctuations far into the bulk, weighed heavily by multiplication with z in its integrand, cause λ not to converge. Contrary, effective medium theory can be used to analyze the total potential drop accross the slab, but any dissection into interfacial and bulk contributions remains ambiguous.[35,70]

Instead of analyzing the EDL width quantitatively, here, we provide a qualitative discussion based on the charge density in subsequent layers. We define the borders of a layer using the zero crossings of the charge density, shown as gray vertical lines in Fig. 3(a). The net charge of each layer, q_i, is calculated by integrating the charge density over that layer. The absolute reduction in charge for each layer, i, on the negative electrode, $|q_{i,cold}| - |q_{i,hot}|$, is plotted in Fig. 3(b), and the relative reduction is plotted in Fig. 3(c). Figure 3(b) shows that the first and second layers of aqueous KCl respond less to temperature changes than the third and fourth layers. Presumably, this is due to the strong solid–liquid and liquid–liquid interactions in these first two layers, associated, for instance, with the 2D-hydrogen bond network at the interface.[66]

The small impact of temperature on the first layer is reminiscent of a Stern layer or a compact layer. Further layers appear to be less strongly bound and have a significantly reduced charge when the temperature increases. This suggests a more diffuse layer. The absolute charge difference decreases in the outer layers, even if the charge reduction in percentage terms increases, as the total charge in these layers is also lower. The layering and the charge differences shown in Fig. 3 suggest a narrower EDL, as the layer charge converges faster toward the bulk value of zero at the hot interface. However, a reduced EDL width would contradict the proposed thermal double-layer expansion.[3,5,7,9,67] Therefore, our results are more consistent with the decreased EDL width found in Ref. 27.

So far, we have analyzed the electrolytic charge density ρ_{el}, with contributions from both the ions and the explicit solvent's partial charges. Implicit solvent models, such as GC and its extensions, treat the solvent as a uniform background, and only ion densities are included. To compare to such implicit solvent models, in the supplementary material, we analyze the electrolytic charge density excluding solvent. In particular, the number of ions in the EDL and their average distance from the electrode are presented (see Sec. S3). The ionic density generally decreases for all electrolytes because the density of the bulk electrolyte decreases with temperature. Nevertheless, the excess charge in the EDL is almost equal to, and opposite to, the applied charge at the electrode, remaining unaffected by temperature. The average distance of the ions from the electrode remains unaffected for KCl and BMIM-PF$_6$ but decreases for TEA-BF$_4$ (see Table S3). However, there are no clear correlations between ion density at the interface and the TVR. This indicates that the effects of the solvent must be included in the description of the EDL to provide an accurate representation.

D. Interfacial permittivity

The generalized permittivity profile is obtained from Eq. (8) Simulations with uncharged electrodes serve here as a reference for the polarization density at both temperatures. Figure 4(a) shows the resulting profile $\varepsilon_\perp^{-1}(z)$ for hot and cold aqueous KCl. Starting from the left of Fig. 4(a), the vacuum close to the electrode results in an inverse generalized permittivity of one, which does not change when the system is heated. Near the electrode, the temperature significantly affects the EDL's generalized dielectric response, i.e., including the effects of ions and solvents. Toward the bulk, fluctuations in the inverse generalized permittivity, which are coupled to the fluctuations in charge in the EDL layers, attenuate, and the inverse permittivity converges to zero in the bulk.

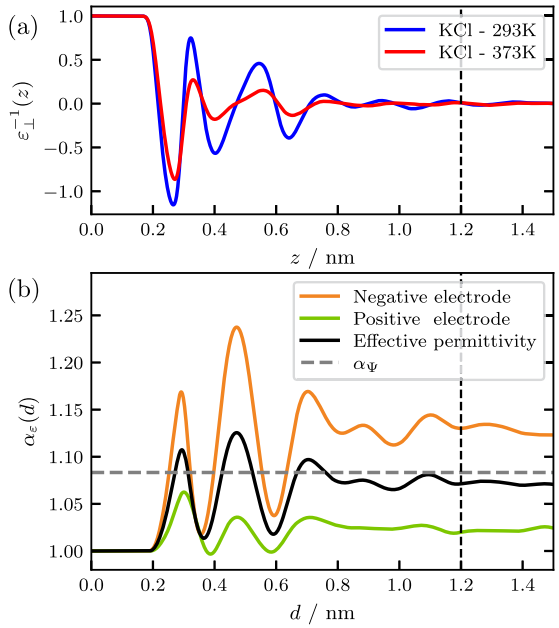

FIG. 4. (a) Permittivity profile of KCl for the cold and hot system at the negative electrode. (b) Influence of temperature on interfacial permittivity at all possible widths, and α_Ψ as comparison.

TABLE I. Interfacial permittivity and its temperature dependence for both electrodes and the effective permittivity, compared to the drop in capacitance α_Ψ. d specifies the interface width used in Eq. (9).

Electrode		KCl d = 1.2 nm	TEA-BF_4 d = 1.7 nm	BMIM-PF_6 d = 6 nm
neg.	ε_{DL}^{cold}	8.4	7.9	29.4
	ε_{DL}^{hot}	7.4	7.5	28.7
	α_ε	113.0%	105.3%	102.5%
pos.	ε_{DL}^{cold}	7.3	10.1	28.2
	ε_{DL}^{hot}	7.2	9.7	28.1
	α_ε	102.0%	103.7%	100.2%
Both	ε_{eff}^{cold}	3.9	4.4	14.4
	ε_{eff}^{hot}	3.6	4.2	14.2
	α_ε^{eff}	107.1%	104.6%	101.3%
	α_Ψ	108.3%	104.8%	101.0%

Table I shows interfacial permittivities as determined by Eq. (9) for the three different electrolytes, at T_{hot} and T_{cold}. By adding the permittivities of both electrodes, like capacitances in series, $1/\varepsilon_{eff} = 1/\varepsilon_{DL,neg} + 1/\varepsilon_{DL,pos}$, we determine the effective permittivity, ε_{eff}, which takes the full capacitor (i.e., both electrodes) into account. Here, we neglect the contribution to the total capacitance made by the bulk, as the ions (which have infinite permittivity) and the solvent (whose permittivity is similar to that of water) effectively make the bulk an ionic conductor. Similar to α_Ψ, we can then introduce a thermal permittivity rise $\alpha_\varepsilon = \varepsilon^{cold}/\varepsilon^{hot}$, which describes the change in permittivity with temperature. Figure 4(b) shows the thermal permittivity rise for KCl. The thermal permittivity rise from the effective interface permittivity (black line) is in good agreement with the TVR (gray line) for an interface width of 1.2 nm. Importantly, in Table I, we see that α_ε^{eff} correlates with α_Ψ for all electrolytes. Although differences between the positive and negative electrode in ε_{DL} are found, we hypothesize that changes in the *effective* interfacial permittivity better explain the changes in the EDL and the resulting TVR than the ionic effects alone.

The difference in interfacial permittivity between electrodes is due to different adsorption of the ions and solvent based on the sign of the surface charge, affecting the potential screening. Since the effect of temperature on interfaces can vary, they should be studied and optimized separately to maximize the overall TVR of the system.

IV. CONCLUSION

We have performed MD simulations to provide a more detailed understanding of the thermal voltage rise (TVR), which is necessary for optimizing supercapacitor systems for thermal energy harvesting. We demonstrated that the TVR of a charged interface can be qualitatively modeled with MD simulations. The layering at the interface becomes less pronounced as the temperature increases, resulting in less effective screening and indicating a reduction in EDL width. To the best of our knowledge, we are the first to quantify the temperature dependence of the EDL by calculating the (generalized) interface permittivity for electrolytes. The temperature-dependent changes in interface permittivity are in good agreement with the TVR of the overall cell, showing that the interface structure of the ions and solvent is required to correctly describe the EDL. Thus, the TVR cannot be explained by the thermal double-layer expansion. Instead, the TVR can be explained by a decrease in interfacial permittivity due to reduced ion adsorption and solvent structuring with increasing temperatures.

Future work could study the molecular origin of the TVR in greater detail, focusing, for instance, on solvent and ion orientation,[68] radial density distributions between different molecular types,[69] hydrogen bonding,[66] and ionic liquid ordering.[70] However, these descriptors do not universally apply to all the different electrolytes studied here. Our objective here was to provide a broader description of the TVR based on permittivity rather than effective length. Nevertheless, studying molecular origins in more detail could serve as an interesting starting point for further research, e.g., studying the temperature dependence of the hydrogen-bond network at the interface under an applied potential. For practical applications of the TCEC, non-equilibrium effects are important because temperature affects both the charging time[15] and the rate of self-discharge[5] for supercapacitors. However, MD simulations usually model the interface at equilibrium; time-dependent effects are often not considered. To create an efficient TCEC, the supercapacitor and cycle parameters must be carefully controlled and investigated. Further work should focus on investigating the influence of porosity, given that the interfacial structure of the electrolyte can change drastically in confinement.

SUPPLEMENTARY MATERIAL

See the supplementary material for an equivalent circuit of the complete cell, the simulation parameters, and an analysis of the ion densities.

ACKNOWLEDGMENTS

M.J. was supported by a FRIPRO grant from The Research Council of Norway (Project No. 345079). This work is funded by the Deutsche Forschungsgemeinschaft (DFG, German Research Foundation) as part of the Excellence Strategy of the Federal Government and the federal states – EXC 3120/1 BlueMat: Water-Driven Materials – 533771286.

AUTHOR DECLARATIONS

Conflict of Interest

The authors have no conflicts to disclose.

Author Contributions

Ole Nickel: Conceptualization (lead); Data curation (equal); Formal analysis (lead); Investigation (lead); Methodology (lead); Validation (equal); Visualization (lead); Writing – original draft (lead); Writing – review & editing (supporting). **Mathijs Janssen**: Conceptualization (equal); Formal analysis (equal); Supervision (supporting); Validation (supporting); Writing – original draft (supporting); Writing – review & editing (supporting). **Alexander Schlaich**: Formal analysis (supporting); Methodology (supporting); Validation (supporting); Writing – review & editing (supporting). **Robert Horst Meißner**: Conceptualization (supporting); Formal analysis (supporting); Funding acquisition (lead); Methodology (supporting); Software (supporting); Supervision (lead); Validation (equal); Writing – original draft (supporting); Writing – review & editing (lead).

DATA AVAILABILITY

The data that support the findings of this study are available from the corresponding author upon reasonable request.

REFERENCES

[1] S. Ahualli, M. M. Fernández, G. Iglesias, A. V. Delgado, and M. L. Jiménez, Environ. Sci. Technol. **48**, 12378 (2014).
[2] A. Härtel, M. Janssen, D. Weingarth, V. Presser, and R. van Roij, Energy Environ. Sci. **8**, 2396 (2015).
[3] J. Kim, S. H. Kim, J. Lee, and J. H. Seol, Appl. Therm. Eng. **217**, 119200 (2022).
[4] M. Janssen, T. Verkholyak, A. Kuzmak, and S. Kondrat, J. Mol. Liq. **371**, 121093 (2023).
[5] Y. Lao, P. Tang, J. Zeng, S. Xu, J. Zhu, Q. Dou, X. Xiao, and X. Yan, ACS Nano **19**, 3895 (2025).
[6] J. Kim, B. Özdoğru, D. P. Finegan, and N. James, Energy Convers. Manage. **357**, 121465 (2026).
[7] B. B. Sales, O. S. Burheim, S. Porada, V. Presser, C. J. N. Buisman, and H. V. M. Hamelers, Environ. Sci. Technol. Lett. **1**, 356 (2014).
[8] Y. S. Ju, Appl. Phys. Lett. **111**, 173901 (2017).
[9] Q. Wang, P. Liu, F. Zhou, L. Gao, D. Sun, Y. Meng, and X. Wang, Molecules **27**, 1239 (2022).
[10] D. Boda, D. Henderson, and K.-Y. Chan, J. Chem. Phys. **110**, 5346 (1999).
[11] V. Lockett, R. Sedev, J. Ralston, M. Horne, and T. Rodopoulos, J. Phys. Chem. C **112**, 7486 (2008).
[12] F. Silva, C. Gomes, M. Figueiredo, R. Costa, A. Martins, and C. M. Pereira, J. Electroanal. Chem. **622**, 153 (2008).
[13] L. Siinor, R. Arendi, K. Lust, and E. Lust, J. Electroanal. Chem. **689**, 51 (2013).
[14] M. Haque, Q. Li, A. D. Smith, V. Kuzmenko, E. Köhler, P. Lundgren, and P. Enoksson, Electrochim. Acta **263**, 249 (2018).
[15] M. Drüschler, N. Borisenko, J. Wallauer, C. Winter, B. Huber, F. Endres, and B. Roling, Phys. Chem. Chem. Phys. **14**, 5090 (2012).
[16] J. Vatamanu, L. Xing, W. Li, and D. Bedrov, Phys. Chem. Chem. Phys. **16**, 5174 (2014).
[17] M. Chen, Z. A. H. Goodwin, G. Feng, and A. A. Kornyshev, J. Electroanal. Chem. **819**, 347 (2018).
[18] F. Angiolari, A. Coretti, M. Salanne, and S. Bonella, Proc. Natl. Acad. Sci. U. S. A. **122**, e2520026122 (2025).
[19] G. Gonella, E. H. G. Backus, Y. Nagata, D. J. Bonthuis, P. Loche, A. Schlaich, R. R. Netz, A. Kühnle, I. T. McCrum, M. T. M. Koper, M. Wolf, B. Winter, G. Meijer, R. K. Campen, and M. Bonn, Nat. Rev. Chem. **5**, 466 (2021).
[20] R. J. Hunter, *Foundations of Colloid Science*, 2nd ed. (Oxford University Press, 2002).
[21] D. Brogioli, Phys. Rev. Lett. **103**, 058501 (2009).
[22] A. Limaye, D. Suvlu, and A. P. Willard, Faraday Discuss. **249**, 267 (2024).
[23] M. F. M. Bijmans, O. S. Burheim, M. Bryjak, A. Delgado, P. Hack, F. Mantegazza, S. Tenisson, and H. V. M. Hamelers, Energy Procedia **20**, 108 (2012).
[24] A. V. Delgado, S. Ahualli, M. M. Fernández, M. A. González, G. R. Iglesias, J. F. Vivo-Vilches, and M. L. Jiménez, Environ. Chem. **14**, 279 (2017).
[25] M. Simoncelli, N. Ganfoud, A. Sene, M. Haefele, B. Daffos, P.-L. Taberna, M. Salanne, P. Simon, and B. Rotenberg, Phys. Rev. X **8**, 021024 (2018).
[26] J. Lin, N. Wu, L. Li, M. Xie, S. Xie, X. Wang, N. Brandon, Y. Sun, J. Chen, and Y. Zhao, Renewable Energy **183**, 283 (2022).
[27] M. Janssen, "The electric double layer put to work," Ph.D. thesis, Utrecht University, 2017.
[28] O. Stern, Z. Elektrochem. Angew. Phys. Chem. **30**, 508 (1924).
[29] J. O. Bockris, M. A. V. Devanathan, and K. Müller, Proc. R. Soc. London, Ser. A **274**, 55 (1963).
[30] D. J. Bonthuis, S. Gekle, and R. R. Netz, Phys. Rev. Lett. **107**, 166102 (2011).
[31] P. Loche, C. Ayaz, A. Wolde-Kidan, A. Schlaich, and R. R. Netz, J. Phys. Chem. B **124**, 4365 (2020).
[32] F. Deißenbeck, C. Freysoldt, M. Todorova, J. Neugebauer, and S. Wippermann, Phys. Rev. Lett. **126**, 136803 (2021).
[33] O. Teschke, G. Ceotto, and E. F. de Souza, Chem. Phys. Lett. **326**, 328 (2000).
[34] L. Fumagalli, A. Esfandiar, R. Fabregas, S. Hu, P. Ares, A. Janardanan, Q. Yang, B. Radha, T. Taniguchi, K. Watanabe, G. Gomila, K. S. Novoselov, and A. K. Geim, Science **360**, 1339 (2018).
[35] P. Stärk, H. Stooß, P. Loche, D. Bonthuis, R. Netz, and A. Schlaich, Chem. Phys. Rev. **7**, 011319 (2026).
[36] D. Boda, D. Henderson, K.-Y. Chan, and D. T. Wasan, Chem. Phys. Lett. **308**, 473 (1999).
[37] J. Reszko-Zygmunt, S. Sokołowski, D. Henderson, and D. Boda, J. Chem. Phys. **122**, 084504 (2005).
[38] M. Alawneh, D. Henderson, C. W. Outhwaite, and L. B. Bhuiyan, Mol. Simul. **34**, 501 (2008).
[39] M. S. Islam, S. Lamperski, M. M. Islam, D. Henderson, and L. B. Bhuiyan, J. Chem. Phys. **152**, 204702 (2020).
[40] A. T. Bui and S. J. Cox, Phys. Rev. Lett. **134**, 148001 (2025).
[41] J. Lin, Z. Zhang, X. Zhu, C. Meng, N. Li, J. Chen, and Y. Zhao, Energy Convers. Manage. **184**, 40 (2019).
[42] C. Cruz and A. Ciach, Molecules **26**, 3668 (2021).
[43] A. P. Thompson, H. M. Aktulga, R. Berger, D. S. Bolintineanu, W. M. Brown, P. S. Crozier, P. J. in't Veld, A. Kohlmeyer, S. G. Moore, T. D. Nguyen, R. Shan, M. J.

Stevens, J. Tranchida, C. Trott, and S. J. Plimpton, Comput. Phys. Commun. **271**, 108171 (2022).
[44]A. Cheng and W. A. Steele, J. Chem. Phys. **92**, 3858 (1990).
[45]L. J. V. Ahrens-Iwers, M. Janssen, S. R. Tee, and R. H. Meißner, J. Chem. Phys. **157**, 084801 (2022).
[46]H. J. C. Berendsen, J. R. Grigera, and T. P. Straatsma, J. Phys. Chem. **91**, 6269 (1987).
[47]S. Deublein, J. Vrabec, and H. Hasse, J. Chem. Phys. **136**, 084501 (2012).
[48]J.-P. Ryckaert, G. Ciccotti, and H. J. C. Berendsen, J. Comput. Phys. **23**, 327 (1977).
[49]M. L. P. Price, D. Ostrovsky, and W. L. Jorgensen, J. Comput. Chem. **22**, 1340 (2001).
[50]J. N. Canongia Lopes and A. A. H. Pádua, Theor. Chem. Acc. **131**, 1129 (2012).
[51]D. Roy and M. Maroncelli, J. Phys. Chem. B **114**, 12629 (2010).
[52]L. J. V. Ahrens-Iwers and R. H. Meißner, J. Chem. Phys. **155**, 104104 (2021).
[53]I.-C. Yeh and M. L. Berkowitz, J. Chem. Phys. **111**, 3155 (1999).
[54]G. Bussi, D. Donadio, and M. Parrinello, J. Chem. Phys. **126**, 014101 (2007).
[55]D. J. Bonthuis, S. Gekle, and R. R. Netz, Langmuir **28**, 7679 (2012).
[56]C. Schröder, M. Haberler, and O. Steinhauser, J. Chem. Phys. **128**, 134501 (2008).
[57]P. Loche, A. Wolde-Kidan, A. Schlaich, D. J. Bonthuis, and R. R. Netz, Phys. Rev. Lett. **123**, 049601 (2019).
[58]A. G. Pandolfo and A. F. Hollenkamp, J. Power Sources **157**, 11 (2006).
[59]M. Rami Reddy and M. Berkowitz, Chem. Phys. Lett. **155**, 173 (1989).
[60]P. J. Gee and W. F. van Gunsteren, Mol. Phys. **104**, 477 (2006).
[61]T. Singh and A. Kumar, J. Phys. Chem. B **112**, 12968 (2008).
[62]X. Wang and S.-P. Feng, Front. Mech. Eng. **3**, 20 (2017).
[63]C. Merlet, B. Rotenberg, P. A. Madden, and M. Salanne, Phys. Chem. Chem. Phys. **15**, 15781 (2013).
[64]R. Dupuis, P.-L. Valdenaire, R. J.-M. Pellenq, and K. Ioannidou, Proc. Natl. Acad. Sci. U. S. A. **119**, e2121945119 (2022).
[65]A. Schlaich, E. W. Knapp, and R. R. Netz, Phys. Rev. Lett. **117**(4), 048001 (2016).
[66]K. Goloviznina, J. Fleischhaker, T. Binninger, B. Rotenberg, H. Ers, V. Ivanistsev, R. Meissner, A. Serva, and M. Salanne, Adv. Mater. **36**, 2405230 (2024).
[67]H. Michel, J. Power Sources **154**, 556 (2006).
[68]J. Seebeck, C. Merlet, and R. H. Meißner, Phys. Rev. Lett. **128**, 086001 (2022).
[69]R. Futamura, T. Iiyama, Y. Takasaki, Y. Gogotsi, M. J. Biggs, M. Salanne, J. Ségalini, P. Simon, and K. Kaneko, Nat. Mater. **16**, 1225 (2017).
[70]C. Merlet, D. T. Limmer, M. Salanne, R. van Roij, P. A. Madden, D. Chandler, and B. Rotenberg, J. Phys. Chem. C **118**, 18291 (2014).